RSC Advances

PAPER

Cite this: *RSC Adv.*, 2021, **11**, 14829

Promoted adsorptive removal of chromium(VI) ions from water by a green-synthesized hybrid magnetic nanocomposite (NFe_3O_4Starch-Glu-NFe_3O_4ED)†

Mohamed E. Mahmoud,[a] Rehab M. El-Sharkawy *[b] and Ghada A. A. Ibrahim[c]

A novel magnetic starch-crosslinked-magnetic ethylenediamine nanocomposite, NFe_3O_4Starch-Glu-NFe_3O_4ED, was synthesized *via* microwave irradiation. The characteristics of the assembled NFe_3O_4Starch-Glu-NFe_3O_4ED nanocomposite were evaluated *via* XRD, FT-IR, TGA, BET, SEM and HR-TEM analyses. Its particle size was confirmed to be in the range 11.25–17.16 nm. The effectiveness of the designed nanocomposite for the removal of Cr(VI) ions was explored using the batch adsorption technique. Equilibrium results proved that the adsorptive removal of the target metal ions from aqueous solution was highly dependent on the optimized experimental parameters. The maximum adsorptive removal percentage values (%*R*) of Cr(VI) ions on NFe_3O_4Starch-Glu-NFe_3O_4ED obtained at pH 2.0 were 85.27%, 91.90%, and 96.47% using 10.0, 25.0, and 50.0 mg L^{-1} Cr(VI), respectively, for an equilibrium time of 30 min. The adsorption process was found to be strongly influenced by the presence of interfering salts including NaCl, $CaCl_2$, KCl, $MgCl_2$, and NH_4Cl. Kinetic studies were performed and it was found that the pseudo-second and Elovich models well fitted the experimental data with the possible suggested ion-pair interaction mechanism. Different isotherm models were employed to assess the adsorption equilibrium, which was revealed by fitting Langmuir, Temkin and Freundlich models. The maximum uptake capacity based on the Langmuir model was 210.741 mg g^{-1}. The effect of temperature and thermodynamics confirmed that adsorption was spontaneous, feasible, and endothermic in nature. Finally, the validity and applicability of using the NFe_3O_4Starch-Glu-NFe_3O_4ED nanocomposite to remove Cr(VI) ions from real water matrices were confirmed in the range of 91.2–94.7 ± 2.2–3.7%.

Received 4th February 2021
Accepted 28th March 2021

DOI: 10.1039/d1ra00961c

rsc.li/rsc-advances

1. Introduction

Water pollution by heavy metal ions, which are introduced into the aquatic sources through industrial effluents, is considered a major environmental problem due to their high toxicity and bio-accumulative nature.[1] Hexavalent chromium species (Cr(VI)) is one of the most dangerous heavy metal pollutants. Even at trace levels, its solubility in water and aqueous solution, mobility, and strong oxidation power make it the most reactive and toxic element available in the environment.[2,3] Cr(VI) oxy-anions ($Cr_2O_7^{2-}$, CrO_4^{2-} and $HCrO_4^-$) are the most predominant forms in which chromium is available in aqueous solution. They are highly soluble and reactive.[4,5] Chromium pollutants originate from different chemical processes including electroplating, catalysis, leather tanning, wood preservation, mining chrome ore, metal cleaning, and corrosion control as well as from some products, such as pigments, and fungicides, and in industries, such as chrome and chrome-magnesite refractories, crafts, ceramics, photography, and glass.[6,7] Chromium is released in the environment through leaking, unsuitable storage and/or improper methods of disposal.[8] The most popular health problems resulting from chromium poisoning are kidney malfunction, bladder cancer, liver problems, and allergic skin diseases.[9–11] According to the United States Environmental Protection Agency (EPA) for drinking water standards, the contaminant level of chromium in water used for drinking should be no more than 0.1 ppm, and this figure includes all forms of chromium that may be available in water.[10] However, the concentration of Cr(VI) in wastewater can reach 50–100 mg L^{-1}. This is over 1000 times more than the recommended concentration.[8,10] Thus, considering the adverse effects of chromium in water on both human health and microorganisms, numerous studies have been focused on developing effective approaches to remove this hazardous species from the aquatic ecosystem.[12]

Numerous techniques have been implemented to remove chromium from water. They mostly involve adsorption,

[a]*Faculty of Science, Chemistry Department, Alexandria University, P.O. Box 426, Ibrahimia, 21321, Alexandria, Egypt*

[b]*Faculty of Dentistry, Chemistry Department, Pharos University in Alexandria, P.O. Box 37, SidiGaber, Alexandria, Egypt. E-mail: rehab.mansour@pua.edu.eg; Tel: +20-1229727752*

[c]*Faculty of Education, Chemistry and Physics Department, Alexandria University, El-Shatby, Alexandria, Egypt*

† Electronic supplementary information (ESI) available. See DOI: 10.1039/d1ra00961c

electrodialysis, photocatalytic remediation, evaporative recovery, chemical reduction, membrane filtration, reverse osmosis, and ion exchange.[13–15] Among the various technologies, adsorption has attracted significant attention from many researchers, considering that it is low-cost, reliable, simple, and highly efficient.[16] The effective adsorptive removal of Cr(VI) from water may be accomplished by biocompatible materials including starch, wheat straw, chitosan, alginate, and cellulose.[3,17–19] Recently, adsorptive remediation combined with magnetic separation has been employed extensively in the industrial field for water purification and other environmental applications.[12] Magnetic separation is efficient, selective, and faster than conventional separation processes, such as centrifugation and filtration.[20] Also, employing magnetic nanoparticles that adsorb metal ions from water has many advantages, including simplicity, effectiveness, recyclability of the magnetic nanosorbent, and the fact that they can be totally removed from solution, preventing their release into the environment, which can cause unknown damage.[21] Magnetic nanoparticles, particularly nanomagnetite (Fe_3O_4 NPs), are well known as efficient nanosorbents. They highly adsorb metal and anionic contaminants, including mercury, chromium, arsenic, selenium, and lead, because of their high surface area to volume ratio, high density of reactive surface sites, low diffusion resistance, good biocompatibility, and low toxicity, in addition to their magnetic properties.[20–23] Furthermore, their crosslinking or grafting with organic molecules, such as polymers, polysaccharides, and biomolecules may improve the adsorption effectiveness of the functionalized nanocomposites.[1,3,12,20,23] Accordingly, it has been found that Fe_3O_4 NP-based nanocomposites are very effective for the quantitative recovery of Cr(VI) with high selectivity. For instance, it was reported that magnetic polypyrrole (PPy)-coated-Fe_3O_4 NPs with a core–shell structure could efficiently remove Cr(VI).[24] Ethylenediamine-modified cross-linked magnetic chitosan resin (EMCMCR) was synthesized and applied for the removal of chromium(VI) ions from aqueous solution using the batch adsorption technique.[25] The adsorption capacities of the prepared nanoadsorbent were found to reach the maximum of 51.813, 48.780, and 45.872 mg g^{-1} at temperatures of 293, 303, and 313 K, respectively. A study was conducted to examine the influence of co-existing ions and natural organic matter on the removal of chromium(VI) from aqueous solution. A nanoscale zero-valent iron (nZVI)–Fe_3O_4 nanocomposite was developed and prepared for this purpose using the *in situ* reduction technique.[26] Adsorption kinetics, isotherm, and thermodynamic studies for the removal of Cr(VI) from wastewater were undertaken using a series of core–shell-structured amino-functionalized Fe_3O_4-NP (NH_2-NMP) magnetic polymer adsorbents linked with various diamino groups, such as triethylenetetramine (TETA), ethylenediamine (EDA), and diethylenetriamine (DETA).[27] Functionalized magnetic graphene nanocomposites (Fe_3O_4–GS) were fabricated for the selective and efficient removal of Pb(II), Hg(II), Cr(VI), Ni(II) and Cd(II). These metals had the sorption capacities of 27.95, 23.03, 17.29, 22.07 and 27.83 mg g^{-1}, respectively.[28] In addition, the effect of the amount of glycidylmethacrylate (GMA) used for the adsorption of metal on the properties of the amino-functionalized nano-Fe_3O_4 magnetic polymer adsorbent (NH_2-NMPs) was investigated for the removal of Cr(VI) from aqueous solution.[29] To efficiently and completely remove Cr(VI) in 5.0 min from wastewater, magnetic graphene nanocomposites decorated with core@double-shell nanoparticles (MGNCs) were synthesized.[30] Also, a magnetic double-base Fe_3O_4@bagasse@chitosan (FBC) aerogel was reported to be an effective adsorbent for the removal of Cr(VI), which exhibited the maximum adsorption capacity of 41 mg g^{-1} at 65 °C.[31]

Natural polysaccharides, such as starch, chitosan, chitin, cellulose, lignin, alginate, and pectin, are polymeric carbon derivatives with numerous practical applications.[32] They have the ability to strongly bind metal ions and can be used for the adsorption of heavy metals.[17–19] Among these biological polymers, starch, with sufficient free hydroxyl groups on its backbone, has received much more attention in the removal of chromium and other heavy metals from aqueous solution due to its high natural abundance, selectivity, biodegradability, biocompatibility, low cost, environmentally friendly nature, and high adsorption efficiency.[33,34] Starch molecules consist of a large number of glucose units linked by glycosidic bonds. To improve the performance of starch as an adsorbent, different functional groups can be easily added to its backbone to target different pollutants. Functionalization can occur *via* specific interactions such as hydrogen bonding, chelating effects, and electrostatic interaction.[33] Many studies have been focused on the use of starch, cross-linked starch and magnetic starch for the adsorption of Cr(VI) ions from aqueous solution.[12,34–38]

The aim of this study is basically directed towards developing a novel hybrid nanocomposite by crosslinking two different nanocomposites, namely starch-For-NFe_3O_4 and NFe_3O_4-For-ED *via* glutaraldehyde using a simple facile microwave-assisted heating approach. The synthesized nanocomposite aimed to combine the chemical properties of magnetite nanoparticles (an efficient and selective nanosorbent with magnetic power), starch (an excellent chelating polymer with biodegradable properties), and ethylenediamine (which contains abundant amino chelating groups to accomplish surface functionalization). The use of microwave-assisted irradiation was also aimed to provide a chemical route for uniform heating, controlled growth rate, uniform nucleation, and facilitating better porosity compared to other conventional thermal processes. Monitoring and optimizing the experimental controlling parameters in the adsorptive removal process of Cr(VI) on the NFe_3O_4Starch-Glu-NFe_3O_4ED nanocomposite together with the kinetics, adsorption isotherm modeling and thermodynamic parameters were intensively investigated in this study. The potential applications of the newly developed nanocomposite for removing Cr(VI) ions from real water matrices were also demonstrated.

2. Experimental procedure

2.1. Materials, reagents, and instrumentation

The chemicals and reagents in this work were of high purity and used as received, as listed in Table S1 (ESI†). In addition, the

specifications of the instruments applied in this study are compiled in Table S2 (ESI†).

2.2. Synthesis of Fe_3O_4 NPs

Fe_3O_4 magnetic nanoparticles were synthesized according to a former study.[39] In this procedure, 50.0 mL HCl solution (0.50 mol L^{-1}) was used to dissolve 0.02 mol $FeCl_2$ and 0.04 mol $FeCl_3$. A microwave oven with a power of 800 W was used to heat the above mixture to 80 °C. Then, a volume of 400 mL of sodium hydroxide (NaOH) (2.0 mol L^{-1}) was added to this solution in four batches with continuous stirring. After each addition, the mixture was heated to 80 °C for one minute in the microwave oven at 800 W. After the final addition, the mixture solution containing the Fe_3O_4 NPs precipitate was inserted back into the microwave and heated for 2.0 min. Following this step, the Fe_3O_4 NPs were separated with the help of a magnet. They were then washed with double distilled water (DDW) several times and left to dry at 50 °C.

2.3. Microwave-assisted preparation of (NFe_3O_4Starch-Glu-NFe_3O_4ED) nanocomposite

The NFe_3O_4Starch-Glu-NFe_3O_4ED nanocomposite was synthesized as follows with the help of three successive microwave-assisted heating stages. Firstly, Fe_3O_4-crosslinked-starch (starch-NFe_3O_4) was prepared *via* the surface reaction of the cross-linked Fe_3O_4 NPs with starch based on the following procedure. Briefly, 4.0 g Fe_3O_4 NPs and 10.0 mL formaldehyde (cross-linking reagent) were mixed in a porcelain dish. The reaction mixture was placed in a microwave oven and heated at 80 °C for 3.0 min. Subsequently, a starch solution was prepared by dissolving 2.0 g of starch in a suitable amount of hot DDW with continuous stirring for 1.0 h and added to the mixture while stirring until a paste was formed. The paste was then dried in the microwave oven at 80 °C for 3.0 min. 10.0 mL of DDW was added to dropwise to the produced material with stirring until a paste was formed, and then irradiated in the microwave oven for another 3.0 min. After three cycles of heating and stirring, the sample was washed with 50.0 mL of DDW to remove any reaction residue and was left to dry at a temperature of 70 °C for 6.0 h. Finally, a mortar and pestle was used to grind the dry product to produce a very fine powder.

In the second stage of this synthetic route, similar steps were performed to produce the (NFe_3O_4-ED) nanocomposite. Briefly, 4.0 g of the synthesized Fe_3O_4 NPs was dispersed in 10.0 mL formaldehyde by stirring in a porcelain dish for 15.0 min. Then 5.0 mL of ethylenediamine was then added dropwise with stirring. Subsequently, the mixture was continuously reacted under microwave irradiation at 80 °C for 3.0 min. Another 5.0 mL of ethylenediamine was introduced to the mixture and again the system was irradiated in the microwave oven for 3.0 min. DDW and ethanol were used to wash the solid product (NFe_3O_4-ED), which was then dried at 70 °C for 6.0 h and finally ground into a very fine powder.

The final synthetic stage was accomplished by crosslinking a combination of the two nanocomposites, starch-NFe_3O_4 and NFe_3O_4-ED, simultaneously using glutaraldehyde as a cross-linker. In detail, 5.0 g of starch-NFe_3O_4 and 5.0 g NFe_3O_4-ED were mixed very well with 20.0 mL glutaraldehyde in a porcelain dish, while stirring for 10.0 min to obtain a paste, which was then irradiated in the microwave oven for 3.0 min. Subsequently, 10.0 mL of distilled water was added dropwise to the above reaction mixture and irradiated in the microwave oven for 3.0 min. This step was repeated three times and finally, DDW and ethanol were used to wash the newly modified hybrid nanocomposite (NFe_3O_4Starch-Glu-NFe_3O_4ED). The mixture was dried at 70 °C until completely dry and ground into a very fine powder. The synthetic route for the preparation of the NFe_3O_4Starch-Glu-NFe_3O_4ED nanocomposite is displayed in Scheme 1.

2.4. Sorption studies of Cr(VI) by NFe_3O_4Starch-Glu-NFe_3O_4ED

The adsorption behavior of Cr(VI) ions on the NFe_3O_4Starch-Glu-NFe_3O_4ED nanocomposite from aqueous solution and real matrices was investigated using the batch adsorption technique at room temperature (25 ± 1 °C). A specific amount of potassium dichromate ($K_2Cr_2O_7$) was dissolved in DDW to prepare a stock solution of Cr(VI) ions (1000.0 mg L^{-1}). Several rounds of successive dilution were performed to obtain the desired concentrations of Cr(VI). The conditions under which adsorption was conducted including solution pH, shaking time, reaction temperature, NFe_3O_4Starch-Glu-NFe_3O_4ED nanocomposite dosage, and the presence of interfering ions were studied and optimized using three different initial Cr(VI) ion concentrations. Metal capacity (q_e; mg g^{-1}) and adsorptive removal percentage (%R) were measured *via* three adsorption experiments and the average value was calculated.

For the study of the effect of pH, an amount of 10.0 ± 1.0 mg of the NFe_3O_4Starch-Glu-NFe_3O_4ED nanocomposite was mixed with 10.0 mL Cr(VI) in an aqueous solution with the following initial concentrations 10.0, 25.0, and 50.0 mg L^{-1} in a 50.0 mL volumetric flask. The initial pH values were adjusted (1.0–7.0) and the pH of the solutions was regulated using either 0.1 M HCl or 0.1 M NaOH. The mixture was automatically stirred using a 250 rpm mechanical shaker for 30.0 min. The magnetic NFe_3O_4Starch-Glu-NFe_3O_4ED nanocomposite, together with the metal ions adsorbed, were pulled out of the mixture using an external magnetic field. It was then washed using 100.0 mL of DDW. The complexing agent 1,5-diphenylcarbazide and a UV-Vis spectrophotometer (in the visible region at wavelength of λ_{max} = 540 cm^{-1}) were used to determine the residual concentration of Cr(VI).[40] The adsorptive removal percentage (%R) and the adsorption capacity (q_e; mg g^{-1}) of Cr(VI) ions on the NFe_3O_4Starch-Glu-NFe_3O_4ED nanocomposite were calculated using eqn (1) and (2), respectively.

$$\%R = \frac{(C_0 - C_t)}{C_t} \times 100 \quad (1)$$

$$q_e = (C_0 - C_t) \times \frac{V}{W} \quad (2)$$

where C_t is the concentration of Cr(VI) ions at equilibrium (mg L^{-1}), C_0 is the initial concentration of Cr(VI) ions before the

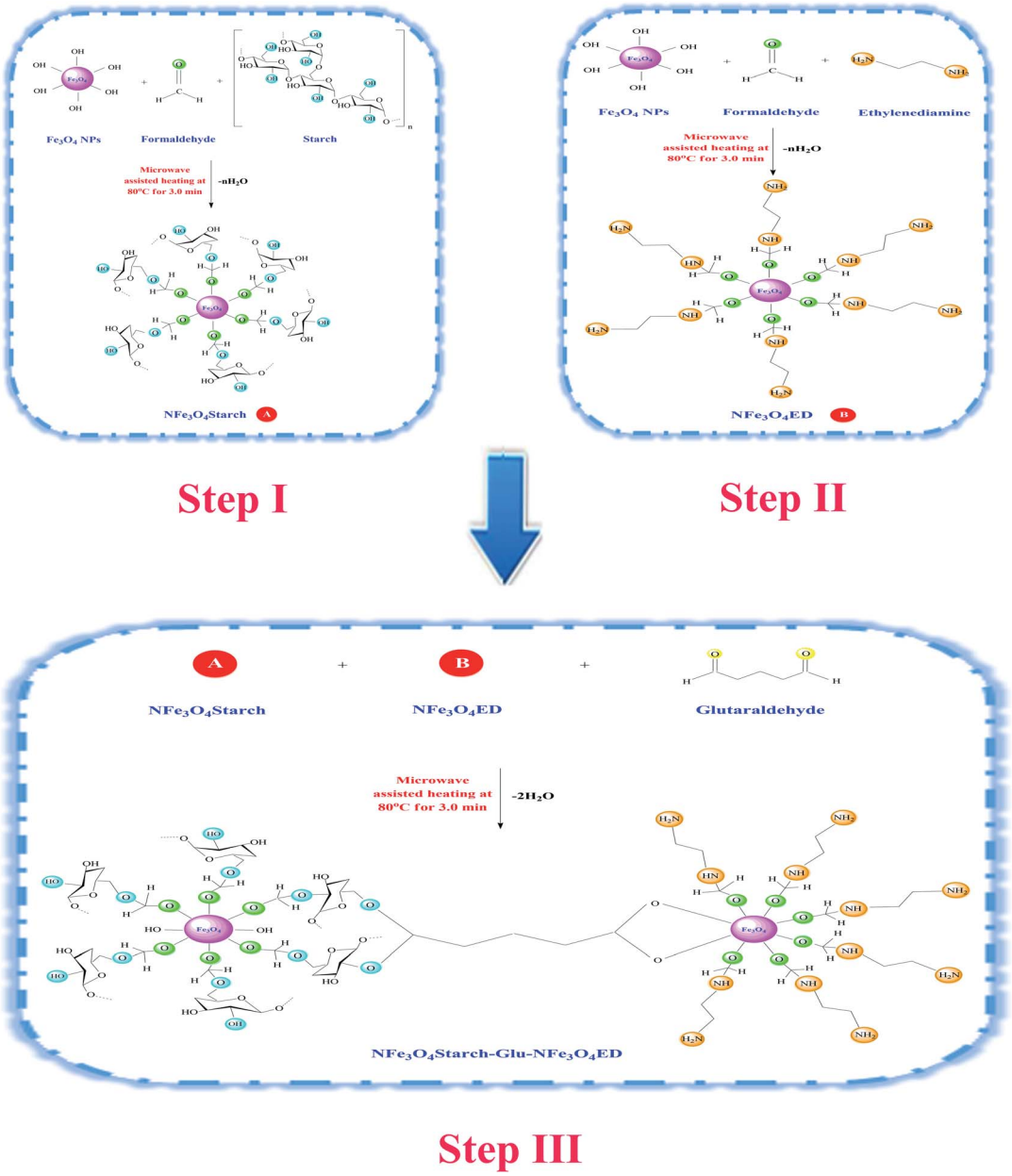

Scheme 1 Synthetic route of the NFe_3O_4Starch-Glu-NFe_3O_4ED nanocomposite.

adsorption process (mg L^{-1}), W is the weight of the nanocomposite (mg) and V is the volume of solution in Liter.

The shaking time and its influence on the removal process of Cr(VI) ions was monitored as follows. In 50.0 mL volumetric flasks, 10.0 mL of Cr(VI) solution (at initial concentrations of 10.0, 25.0, and 50.0 mg L^{-1}) was added to 10.0 ± 1.0 mg nanocomposite and the pH of solution was adjusted to its identified optimum value, which was obtained from the previous step (pH = 2.0). The shaking times were set at 1.0, 5.0, 10.0, 15.0, 20.0, 30.0, 40.0, 50.0, and 60.0 min using a 250 rpm automatic shaker at room temperature. Then, an external magnetic field was used to separate the magnetic nanocomposite together with the adsorbed Cr(VI) metal ions from solution. The remaining Cr(VI) ions were identified at the maximum absorbance (λ = 540 cm^{-1}), as mentioned before. Finally, the adsorptive removal percentage (%R) values were determined using eqn (1). The investigated time factor was used to conduct the kinetic studies and determine the adsorption models applied to explain the interaction mechanism(s) between Cr(VI) ions and the NFe_3O_4Starch-Glu-NFe_3O_4ED nanocomposite. The models tested were the *pseudo*-first-order, *pseudo*-second order, intra-particle diffusion and Elovich models. Table S3 (ESI†) presents more details about the definition and parameters of the kinetic models.

The mass optimization of the NFe_3O_4Starch-Glu-NFe_3O_4ED nanocomposite was studied for the removal process of Cr(VI) by similar batch experiments using various masses (2.0, 5.0, 10.0, 15.0, 20.0, 30.0, 40.0, 50.0, 75.0 and 100.0 ± 0.1 mg). Typically,

under the optimum conditions of pH and shaking time (2.0 and 30.0 min, respectively), 10.0 mL of different initial Cr(VI) concentrations (10.0, 25.0, and 50.0 mg L^{-1}) were added to the selected nanocomposite mass. The same steps for adsorption and method to calculate the adsorptive removal percentage (%*R*), explained above were followed.

The isotherm studies and sorption equilibrium were evaluated using various initial metal ion concentrations. Specifically, different initial Cr(VI) concentrations ranging from 10.0–100.0 mg L^{-1} were prepared. Then 10.0 mL of each concentration was mixed with 10.0 ± 1.0 mg of NFe_3O_4Starch-Glu-NFe_3O_4ED nanocomposite, the pH and shaking time of the solution were set to their optimum values and the steps were completed as previously explained. After equilibrium, the q_e values were calculated using eqn (2) and Origin Pro 8.5 was used to compute the different isotherm models using the collected data. The isotherm model equations and parameters are listed in Table S4 (ESI).†

Different reaction temperatures (20 °C, 30 °C, 40 °C, 50 °C, and 60 ± 1 °C) were used to conduct the sorption experiments to investigate the effect of reaction temperature on the adsorption process of Cr(VI) and to calculate the thermodynamic parameters. 10.0 mL of Cr(VI) solution (10.0, 25.0 and 50.0 mg L^{-1}, pH 2.0) was mixed with 10.0 ± 1.0 mg of NFe_3O_4Starch-Glu-NFe_3O_4ED. This mixture was shaken at the selected temperatures for 30.0 min with the help of a digital temperature control shaker. The remaining concentration of Cr(VI) ions was determined as illustrated before. To identify the affinity of the NFe_3O_4Starch-Glu-NFe_3O_4ED nanocomposite for Cr(VI), the Gibbs free energy (ΔG°), enthalpy (ΔH°) and entropy (ΔS°) (thermodynamic parameters) were investigated. To calculate these parameters, the data obtained from the reaction temperature factor and the best fitting isotherm model were used.

The ability of NFe_3O_4Starch-Glu-NFe_3O_4ED to extract Cr(VI) in the presence of other interfering ions was tested by mixing 10.0 ± 0.1 mg of the nanocomposite with 100.0 ± 0.1 mg of selected interfering salts (KCl, NaCl, $MgCl_2$, $CaCl_2$, and NH_4Cl) and 10.0 mL Cr(VI) (10.0, 25.0, and 50.0 mg L^{-1}, pH = 2.0). The effect on the adsorption process of Cr(VI) was investigated using the same experimental steps as listed above. As in the previous tests, eqn (1) was used to calculate the adsorptive removal percentage (%*R*).

The potential applications of the NFe_3O_4Starch-Glu-NFe_3O_4ED nanocomposite to remove Cr(VI) ions from different sources of real water matrices including samples of wastewater, tap water and sea water were investigated under the optimized experimental conditions. The wastewater, tap water and sea water samples were collected from El-Mahmoudia Canal, a source of drinking water, and the Mediterranean Sea in Alshatby Area. All sources are located in Alexandria, Egypt. The pH value of the tested water samples was adjusted to pH 2.0 and spiked with the desired concentrations of Cr(VI) (10.0, 25.0 and 50.0 mg L^{-1}). Then, 10.0 mL of each water sample was added to 40.0 ± 1.0 mg of the NFe_3O_4Starch-Glu-NFe_3O_4ED nanocomposite and the reaction mixture was automatically shaken for a period of 30.0 min. Subsequently, the sorbed Cr(VI) ions were separated as previously described and the remaining ions in solution were calculated, as mentioned above. These steps were repeated three times and the average were taken and used to identify the adsorptive removal percentage (%*R*) of Cr(VI) ions according to eqn (1), for each of the three water samples. Blank water samples were used for comparison.

3. Results and discussion

3.1. Structural characterization of (NFe_3O_4Starch-Glu-NFe_3O_4ED)

3.1.1 FT-IR spectroscopy. The FT-IR analysis was generally used to confirm the successful assembly of the target NFe_3O_4-Starch-Glu-NFe_3O_4ED hybrid nanocomposite (Fig. 1). Fig. 1 illustrates different peaks, corresponding to the functional groups of the constituents of the nanocomposite, *e.g.*, Fe_3O_4 NPs, starch, ethylenediamine, and the crosslinking materials. A broad band can be seen at 3271.77 cm^{-1}, which is mainly present because of the intramolecular hydrogen bonding in the magnetic nanocomposite and/or the N–H stretching vibration of the NH_2 group of ethylenediamine.[39] The weak peak at 1714.39 cm^{-1} is assigned to the –OH bending vibration ($\delta_{(OH)}$).[39,41] The two other weak bands observed at 2928.30 and

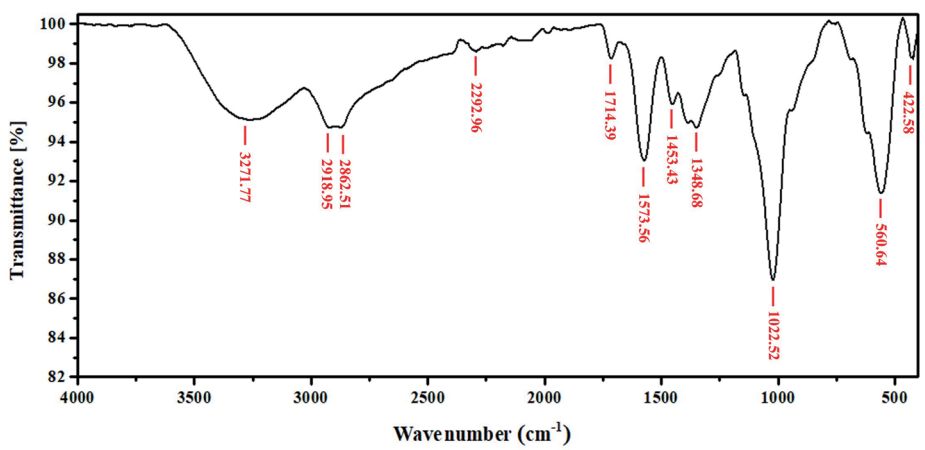

Fig. 1 FT-IR spectrum of the NFe_3O_4Starch-Glu-NFe_3O_4ED nanocomposite.

2862.51 cm^{-1} may be due to the presence of CH_2 and its symmetric and asymmetric stretching vibrations, which is found in starch, glutaraldehyde, and ethylenediamine.[12,42,43] Besides, the medium peak observed at 560.64 cm^{-1} is related to the Fe–O bond of the magnetite nanoparticle phase.[41,42] Another characteristic adsorption band at 422.58 cm^{-1} was clearly seen, which corresponds to the Fe–O–C bond, resulting from the chemical interaction between magnetite nanoparticles and the carbonyl group of the formaldehyde cross-linker.[39,41] In addition, the stretching modes of C–C and C–O present in starch, specifically in its polysaccharide backbone, are represented in the strong peak identified at 1022.52 cm^{-1}.[12,44] The weak band at 1714.39 cm^{-1} and the medium band at 1573.56 cm^{-1} refer to the stretching vibrational modes of NHCO and confirm the formation of amide due to the bonding of ethylenediamine with formaldehyde.[25,42] Furthermore, the weak band at 2292.96 cm^{-1} corresponds to the stretching and bending bands of N–H and free NH_2 in ethylenediamine, respectively.[25,27] Two other peaks are clear in the FT-IR spectrum at 1348.68 cm^{-1} and 1453.43 cm^{-1}. They are both caused by C–H symmetric bending in the H–C–H bending mode of alkane in the structure of the starch molecule.[12,44]

Finally, it is worth noting from the FT-IR analysis that the magnetite, starch, and ethylenediamine present in the nanocomposite matrix interact based on covalent bonding between starch or ethylenediamine and magnetite nanoparticles, using formaldehyde as a cross-linking reagent to produce the NFe_3O_4Starch and NFe_3O_4ED nanocomposites. Besides, the bifunctional glutaraldehyde was found to cross-link these nanocomposites *via* chemical bonding to produce the desired (NFe_3O_4Starch-Glu-NFe_3O_4ED) nanocomposite. Consequently, certain characterized functional groups in the FT-IR spectrum of the NFe_3O_4Starch-Glu-NFe_3O_4ED nanocomposite are directly responsible for its ability to bind and adsorb Cr(VI) from aqueous solutions.

3.1.2. X-ray diffraction (XRD). Fig. S1 (ESI†) displays the X-ray diffractogram of NFe_3O_4Starch-Glu-NFe_3O_4ED, which indicates the amorphous structure of this nanocomposite given that no sharp peaks can be seen. The diffractogram reveals some weak XRD peaks at $2\theta = 30.29°$, 35.72°, 43.36°, 54.40°, 85.71° and 63.93°. These diffraction peaks are related to and indexed according to their corresponding Miller indices, *i.e.*, (220), (311), (400), (422), (511), and (440), respectively. These results imply that Fe_3O_4 NPs are present in the matrix of the assembled nanocomposite.[39,41] Conversely, the wide amorphous diffraction peak observed at $2\theta = 25.69°$ can be ascribed to the presence of starch in the nanocomposite.[44] It is evident from the XRD peaks that the constituents of both Fe_3O_4 NPs and starch are present in the NFe_3O_4Starch-Glu-NFe_3O_4ED nanocomposite. However, the absence of peaks corresponding to ethylenediamine and the cross-linking materials is mainly related to the inability of X-ray diffraction instrumentation to detect them.

3.1.3. Thermal gravimetric analysis (TGA). TGA was performed on the NFe_3O_4Starch-Glu-NFe_3O_4ED nanocomposite to evaluate its thermal stability in the temperature range of 25 °C to 800 °C, as illustrated in Fig. S2 (ESI†). It is noted from the thermogram that the nanocomposite exhibited five successive stages of mass degradation with an overall weight loss of 70.15 wt%. The first stage was identified at 25.56–156.82 °C (loss = 2.09%) due to the possible evaporation of adsorbed water from the surface of this nanocomposite.[44] The second thermal decomposition stage was characterized in the temperature range of 156.82–400.89 °C with 26.19% weight loss. The third thermal decomposition stage was initiated at around 400.89 °C and extended to 545.13 °C. During this thermal process, the sample lost 14.07% of its weight. These two stages are mainly due to the partial and almost complete degradation of the organic moieties from starch and ethylenediamine as well as the cross-linked chains of the formaldehyde and glutaraldehyde portions of NFe_3O_4Starch-Glu-NFe_3O_4ED that resulted in decomposition of various functional groups to gases, such as CO_2, O_2, CH_4, N_2, NH_3, and H_2O.[39,44] The fourth thermal degradation stage was identified at the temperature range of 545.13–713.28 °C with a weight loss of 14.94%. This mainly corresponds to the complete degradation of all the organic compounds in the assembled nanocomposite. The last stage of thermal degradation was observed above 713.28 °C, where the sample exhibited a very small weight loss of only 1.24%, indicating that nanocomposite was finally converted into carbon and the stable iron oxides.[44] The total loss of the last four degradation steps is 56.43% which gives a good indication for the assembly of the nanocomposite and identify the content of loaded organic moiety on the surface of magnetic nanoparticles.

3.1.4. Morphological study using SEM and HR-TEM. The microstructure and surface morphology of the synthesized NFe_3O_4Starch-Glu-NFe_3O_4ED nanocomposite were examined *via* SEM and HR-TEM and the related images are displayed in Fig. 2. The SEM image of the nanocomposite (Fig. 2a) shows that it possesses a rough and porous surface embedded with spherical nanoparticles of Fe_3O_4, monodispersed and uniformly distributed with an average particle size in the range of 18.66–23.50 nm. This surface morphology provides clear evidence of the efficient cross-linking reaction between the components of the nanocomposite. In addition, the SEM image shows that the surface of the NFe_3O_4Starch-Glu-NFe_3O_4ED nanocomposite possesses abundant pores, which can act as active sites to enhance the adsorption of Cr(VI) ions. The HR-TEM image of the NFe_3O_4Starch-Glu-NFe_3O_4ED nanocomposite (Fig. 2b) shows similar results to that concluded from the SEM analysis, with a small difference in particle size. As can be seen, the HR-TEM image of the nanocomposite exhibits dark areas with elliptical to roughly spherical-shaped particles, in addition to light areas. These dark areas correspond to Fe_3O_4 NPs, with a particle size identified in the range of 11.25–17.16 nm. Conversely, the light areas are ascribed to the organic part of the nanocomposite matrix (starch, ethylenediamine and the cross-linkers). Consequently, the SEM and HR-TEM analyses confirm the successful preparation of the newly designed NFe_3O_4Starch-Glu-NFe_3O_4ED nanocomposite.

3.1.5 Surface area analysis. The Brunauer–Emmett–Teller (BET) isotherm method was used to evaluate the surface area and porosity of the assembled NFe_3O_4Starch-Glu-NFe_3O_4ED hybrid nanocomposite. Furthermore, the pore size distribution

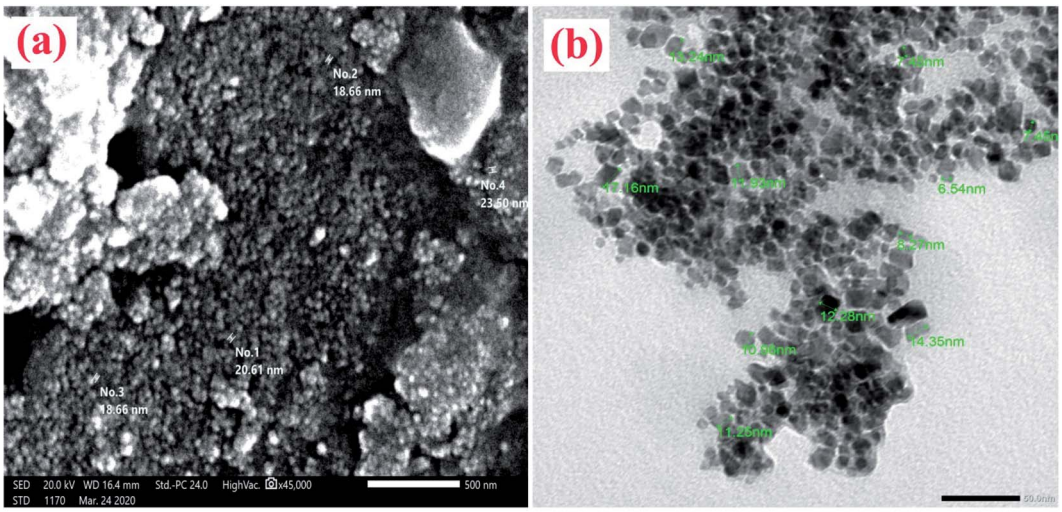

Fig. 2 (a) SEM and (b) HR-TEM images of the NFe_3O_4Starch-Glu-NFe_3O_4ED nanocomposite.

of the nanocomposite was investigated using the Barrett–Joyner–Halenda (BJH) method. Fig. 3 shows the corresponding nitrogen adsorption–desorption isotherms of the nanocomposite. The nanocomposite exhibited a type IV isotherm, as can be seen from the BET isotherm curve. This means that it is a typical mesoporous material, with a type H3 hysteresis loop associated with capillary condensation in the mesopores.[45] The surface area and total pore volume ($P/P_0 = 0.990$) of the NFe_3O_4Starch-Glu-NFe_3O_4ED nanocomposite, which were identified using the BET method and measured at standard temperature and pressure (STP), were found to be 3.134 $m^2\ g^{-1}$ and 3.757×10^{-3} $cm^3\ g^{-1}$, respectively. The mean pore diameter of the nanocomposite was found to be 4.744 nm, which was calculated using the Barrett–Joyner–Halenda (BJH) method. This value proves that the structure of the nanocomposite is mesoporous, and it has a uniform size.[46] This feature offers an increased number of active essential sites to adsorb metal ions, such as Cr(VI), resulting in an enhanced adsorptive removal percentage (%R).

3.2. Adsorption studies

3.2.1. The effect of pH. The pH of the contact solution during the adsorption of Cr(VI) ions by the newly designed (NFe_3O_4Starch-Glu-NFe_3O_4ED) nanocomposite was examined in this study, considering that it is a main factor in the removal process. Generally, the initial pH of the contact solution affects the surface properties of the nanocomposite, such as surface charge, active sites, and solubility. In addition, the pH has a significant influence on the adsorbed metal ions and degree of ionization. Possible reasons for this include hydrolysis and complexation with the functional groups of the nanocomposite.[45,46] Thus, different initial pH values of contact solutions (1.0–7.0) were applied to test the amount of metal taken by the nanocomposite under these conditions. The study was carried out using three different Cr(VI) concentrations (10.0, 25.0, and 50.0 mg L^{-1}) at 25 ± 1.0 °C. Fig. S3 (ESI†) shows the values of %R of Cr(VI) ions by the NFe_3O_4Starch-Glu-NFe_3O_4ED nanocomposite and the effect of the initial pH of contact solution on this process. According to this plot, it can be seen that the adsorption of Cr(VI) ions increased as the pH of the contact solution increased from 1.0 to 2.0, with maximum adsorption observed at pH 2.0. For an initial concentration of 10.0 mg L^{-1}, the maximum %R was 79.38% and 83.82% (25.0 mg L^{-1}), and for 50.0 mg L^{-1}, it reached 82.92%. While, a gradual decrease in the Cr(VI) adsorptive removal percentage values was evident and characterized upon increasing the pH value of contact solution from 3.0 to 7.0. This trend can be best explained considering two facts, one is related to the surface charge of the NFe_3O_4Starch-Glu-NFe_3O_4ED nanocomposite and the other is related to the form of Cr(VI) ions present in the aqueous solution. Generally, in aqueous solutions, Cr(VI) is present in various forms, depending on the pH of the solution. H_2CrO_4 is the form of Cr(VI) when pH = 1.0. For pH in the range

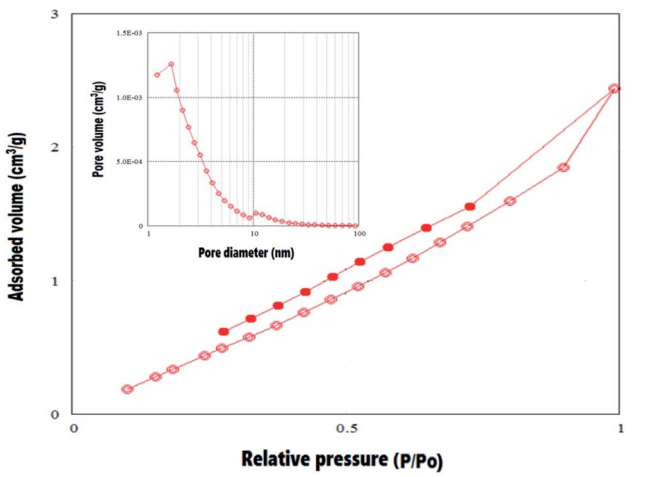

Fig. 3 Nitrogen adsorption–desorption isotherm (inset) pore size of the NFe_3O_4Starch-Glu-NFe_3O_4ED nanocomposite.

of 1.0 to 6.0, $HCrO_4^-$ is the predominant form, while $Cr_2O_7^-$, $Cr_3O_{10}^{2-}$, $HCrO_4^-$, and $Cr_4O_{13}^{2-}$ are also present. With an increase in pH, these forms are turned into CrO_4^{2-} and $Cr_2O_7^{2-}$.[11] Simultaneously, the surface of NFe_3O_4Starch-Glu-NFe_3O_4ED is characterized by the presence of numerous amine ($-NH_2$) and hydroxyl (–OH) active functional groups. The form of these groups differs depending on the pH level. When the pH of the solution is more acidic (<4), these functional groups are easily protonated, thus becoming cationic ($-NH_3^+$ and $-OH_2^+$). This leads to greater attraction to the negatively charged ions present in the solution. Thus, the nanocomposite became electrostatically attracted to $HCrO_4^-$ ions and the removal rates were elevated.[12] When the pH was less than 2, a decrease in the %*R* was recorded as Cr(VI) is available in the form of H_2CrO_4, and chromium and protons compete to bind to the available adsorption sites on the nanocomposite.[14,25] With an increase in the pH value from 3.0 to 7.0, the concentration of H^+ ions decreases, while the $-NH_2$ and –OH are more difficult to protonate. In this case, the concentration of OH^- also increases and it starts to compete with $HCrO_4^-$ on adhering to the surface of the NFe_3O_4Starch-Glu-NFe_3O_4ED nanocomposite, where OH^- prevails, leading to less adsorption of Cr(VI).[27] Thus, it can be concluded that a pH value of 2.0 represents the optimum pH value for the adsorption of Cr(VI) from aqueous solution.

3.2.2. Shaking time factor and kinetic studies. Fig. 4 shows the %*R* of Cr(VI) by the NFe_3O_4Starch-Glu-NFe_3O_4ED nanocomposite considering different shaking contact times using various initial concentrations of Cr(VI) ions, namely, 10.0, 25.0, and 50.0 mg L^{-1}. The adsorption rate of Cr(VI) on NFe_3O_4Starch-Glu-NFe_3O_4ED was initially quite high (from 1.0 to 15.0 min), and then gradually reached equilibrium at 30.0 min. The %*R* of Cr(VI) using a shaking time of 1.0 min was characterized as 53.42%, 61.81% and 57.80% for 10.0, 25.0, and 50.0 mg L^{-1} of Cr(VI), respectively, and these adsorption values reached the maximum at 30.0 min as 79.45% (10 mg L^{-1}), 83.79% (25 mg L^{-1}) and 82.90% (50 mg L^{-1}). The high %*R* after a period of time may have resulted from the complete and more efficient binding between Cr(VI) ions and the active surface sites on the NFe_3O_4Starch-Glu-NFe_3O_4ED nanocomposite.[27] The equilibrium process reached the optimum condition once all the active sites on the nanocomposite were fully occupied by Cr(VI) ions.[37]

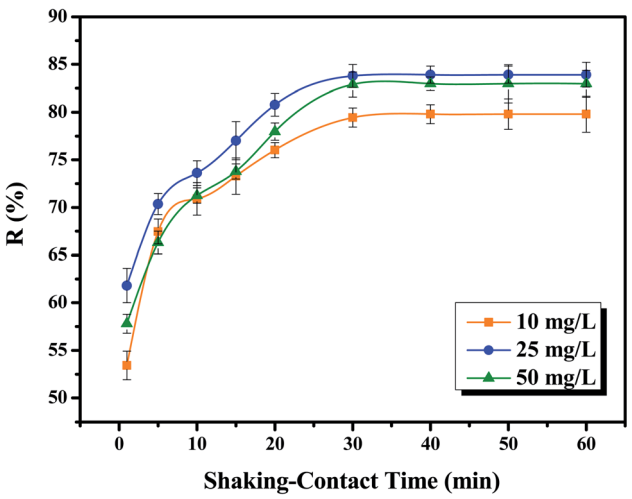

Fig. 4 Effect of contact time on Cr(VI) ion removal percentage (%*R*) by the NFe_3O_4Starch-Glu-NFe_3O_4ED nanocomposite. (Sample volume = 10.0 mL; nanosorbent dose = 10.0 ± 1.0 mg; Cr(VI) initial concentrations = 10.0, 25.0, and 50.0 mg L; pH value = 2.0; shaking time = 1.0, 5.0, 10.0, 15.0, 20.0, 30.0, 40.0, 50.0, and 60.0 min; temperature = 25 °C; shaking speed = 250 rpm).

The use of kinetic models was employed for the analysis of the experimental data to determine the adsorption mechanism and its potential rate-controlling steps, including mass transport and chemical reaction. It is necessary to gather information on the kinetics of metal adsorption to choose the best conditions to apply during the uptake of the metal by the nanocomposite.[28] Thus, to find out the most suitable adsorption mechanism(s) in this research, the following kinetic models were applied to the experimental data for Cr(VI) sorption on NFe_3O_4Starch-Glu-NFe_3O_4ED with different initial Cr(VI) concentrations (10.0, 25.0 and 30.0 mg L^{-1}), pH = 2.0 and at 25 °C, including the pseudo-first order, pseudo-second order, Elovich and intra-particle diffusion models. The equations used to describe these kinetic models and their identified parameters are presented in Table S3 (ESI†). The graphical representations of the investigated kinetic models are illustrated in Fig. S4a–d (ESI†), respectively. The correlation coefficient (R^2) and the predicted q_e values are the two criteria used to validate the order of the adsorption process and estimate the applicability of the kinetic model, respectively. According to the listed values of R^2 and q_e in Table S3 (ESI†), the pseudo-first order (R^2 = 0.9280 for 10.0 mg L^{-1}, 0.8820 for 25.0 mg L^{-1}, and 0.8180 for 50.0 mg L^{-1}; q_e = 3.3906 for 10.0 mg L^{-1}, 10.6867 for 25.0 mg L^{-1}, and 29.1659 for 10.0 mg L^{-1}) (Fig. S4a, (ESI†)) and intra-particle diffusion (R^2 = 0.8940 for 10.0 mg L^{-1}, 0.8700 for 25.0 mg L^{-1}, and 0.8070 for 50.0 mg L^{-1}, Fig. S4b (ESI†)) models provide poor fits for the adsorption process in this study. Consequently, the validity of these models is inadequate for the purpose of interpreting the assumed mechanism of adsorption of Cr(VI) on NFe_3O_4Starch-Glu-NFe_3O_4ED. Conversely, the characterized R^2 and q_e values calculated using the pseudo-second-order kinetic model (R^2 = 0.9999, 0.9996, and 0.9998 and q_e = 8.1967, 21.7391, and 42.6076 for 10.0, 25.0, and 50.0 mg L^{-1}, respectively, Fig. S4c (ESI†)) represent an outstanding fit to the practical data points. This indicates that the pseudo-second-order is the best model to predict the adsorption process from a kinetic point of view, and that it has chemisorption characteristics.[45] Therefore, the possible chemical reactions of Cr(VI) with NFe_3O_4Starch-Glu-NFe_3O_4ED are mainly accomplished by the suggested ion-pair interaction mechanism between Cr(VI) and the hydrogen ions located on the surface of the NFe_3O_4Starch-Glu-NFe_3O_4ED nanocomposite. The same conclusion was deduced concerning the fit of the pseudo-second order model to the adsorption process in other studies using different adsorbents.[25,37,47] Besides, the identified R^2 values for the Elovich model (Fig. S4d, (ESI†)), which is usually applied to describe adsorption on highly heterogeneous surfaces, were found to be 0.9700, 0.9700, and 0.9680 using 10.0, 25.0 and 50.0 mg L^{-1} Cr(VI) ions concentrations, respectively. These good correlation coefficients greatly suggest that

the surface of NFe_3O_4Starch-Glu-NFe_3O_4ED corresponds to a heterogeneous system.[45] Furthermore, the values of the adsorption rate (α) in the Elovich model were characterized as 2916.4027, 50 100.6158, and 14 539.1641 mg g^{-1} min^{-1} for 10.0, 25.0, and 50.0 mg L^{-1} Cr(VI) ion concentrations, respectively, which indicate very rapid and efficient adsorption behavior for the NFe_3O_4Starch-Glu-NFe_3O_4ED nanocomposite.

3.2.3. Effect of NFe_3O_4Starch-Glu-NFe_3O_4ED nanocomposite dosage. Generally, the lower consuming of the adsorbent material is profitable due to the economical consideration. Thus, to calculate the optimum quantity of NFe_3O_4-Starch-Glu-NFe_3O_4ED nanocomposite for the adequate adsorption of Cr(VI), several dosages of NFe_3O_4Starch-Glu-NFe_3O_4ED were used (2.0–100.0 mg) for three different Cr(VI) ion concentrations (10.0, 25.0, and 50.0 mg L^{-1}). The results of these experiments are depicted in Fig. S5 (ESI†) to show that the %R of Cr(VI) increased with an increase in NFe_3O_4Starch-Glu-NFe_3O_4ED nanocomposite dosage until an equilibrium state was reached in the range of 50.0–100.0 mg. The minimum adsorptive removal percentages of Cr(VI) were identified as 52.74%, 40.76%, and 33.61% using 2.0 mg of the NFe_3O_4Starch-Glu-NFe_3O_4ED nanocomposite for the Cr(VI) concentrations of 10.0, 25.0, and 50.0 mg L^{-1}, respectively. The maximum adsorptive removal percentages of Cr(VI) were 85.96%, 92.41%, and 96.47% at 100.0 mg of the nanocomposite for the same concentrations (10.0, 25.0, and 50.0 mg L^{-1}, respectively). This behavior is basically due to the possible increase in the number of active functional groups that are freely available to interact with the target metal ions on the surface of the NFe_3O_4Starch-Glu-NFe_3O_4ED nanocomposite in the same volume and therefore increase the efficiency of adsorption.[42,43]

3.2.4 Adsorption isotherm study using the effect of the concentration of Cr(VI) ions on NFe_3O_4Starch-Glu-NFe_3O_4ED. To explain the mechanism of interaction between the adsorbing solid material of the nanocomposite and metal ions, adsorption isotherms were applied to determine the equilibrium between the concentration of metal ions remaining in the solution (C_e) and the amount that was already adsorbed on the surface of the nanocomposite (q_e). Accordingly, the adsorption isotherms can describe the equilibrium distribution of adsorbed molecules (Cr(VI) ions) between the solid NFe_3O_4Starch-Glu-NFe_3O_4ED nanocomposite and liquid phases. Varying the initial metal ions concentration is the most commonly known procedure to evaluate the isotherm parameter adsorbent-adsorbate system. Mostly, the metal adsorption equilibrium should be reached when its concentration in bulk liquid phase is in a balance with that at the boundaries of solid phase.[44] The experimental equilibrium data for the adsorption of Cr(VI) on the NFe_3O_4-Starch-Glu-NFe_3O_4ED nanocomposite was described by four models of adsorption isotherms, Freundlich, Langmuir, Temkin, and Dubinin–Radushkevich (D–R) using different initial concentrations of Cr(VI) ions (10.0–100.0 mg L^{-1}) at 25 °C, where the pH was 2.0. Table S4 and Fig. S6a–d (ESI†) show the linear equations of the isotherm models studied and the parameters calculated for the sorption process in this work. It can be concluded from Fig. S6a (ESI†) that the Langmuir plot best describes the sorption process with $R^2 = 0.9501$. Thus, this verified that Cr(VI) ions covered the surface of NFe_3O_4Starch-Glu-NFe_3O_4ED in a monolayer distribution. The maximum identified value for Cr(VI) adsorption capacity by the NFe_3O_4Starch-Glu-NFe_3O_4ED nanocomposite, q_{max}, was 210.741 mg g^{-1} (Table S4, (ESI†)). In addition, the identified K_L (Langmuir constant) value (0.0274) refers to the favorable adsorption reaction between Cr(VI) and NFe_3O_4Starch-Glu-NFe_3O_4ED at pH 2.0. The other essential characteristic parameter of the identified isotherm, namely the Langmuir isotherm, is the dimensionless constant separation factor or equilibrium parameter (R_L), which can be calculated using eqn (3) as follows:[25]

$$R_L = \frac{1}{1 + K_L C_0} \quad (3)$$

where C_0 (mg L^{-1}) is the initial concentration of the target metal ions and K_L (L mg^{-1}) is the Langmuir constant. Table S4 (ESI†) shows the calculated value of R_L. Generally, the value of R_L is always <1 when the Langmuir isotherm model is fitted.[44] As can be seen in Table S4 (ESI†), the values R_L were identified to be in the range of 0.2676–0.6463.

The Freundlich isotherm assumes that adsorption occurs on a heterogeneous nanocomposite surface, which affords unequal free active binding sites with various energies of adsorption. This is represented by an empirical equation and the adsorption capacity in this case is related to the concentration of Cr(VI) at equilibrium (C_e). The linear equations and the calculated isotherm parameters for the Freundlich isotherm model are presented in Table S4 (ESI†). The identified value of R^2 of this isotherm model (0.9340), as given in Table S4 and Fig. S6b (ESI†), denotes that the Freundlich model is less favorable for the explanation of the adsorption of Cr(VI) on NFe_3O_4Starch-Glu-NFe_3O_4ED. However, the sorption intensity constant (n) for this adsorption system was found to be greater than unity, confirming the favorable sorption process by the NFe_3O_4Starch-Glu-NFe_3O_4ED nanocomposite. This is because the higher the n-value ($n > 1$), the higher the intensity of sorption.[44] Besides, the characterized value of the Freundlich constant, K_F, (6.117 L mg^{-1}) also indicates the high adsorption capacity of the NFe_3O_4Starch-Glu-NFe_3O_4ED nanocomposite.

In the case of the Temkin isotherm,[48] it assumes that the heat emitted throughout the adsorption process decreases in a linear manner as more of the nanocomposite is covered by the adsorbate given that they both interact. This isotherm can predict whether this process is physically or chemically controlled. The calculated parameters by the linear form of Temkin model are illustrated in Table S4 (ESI†). Eqn (4) was used to calculate the Temkin isotherm equilibrium constant (b_T; measured in kJ mol^{-1}). This constant is an expression of the heat of adsorption and/or the adsorption bonding energy.

$$b_T = \frac{RT}{B} \quad (4)$$

where B is the Temkin constant, R is the gas constant (8.314×10^{-3} kJ mol^{-1} K^{-1}) and T is the absolute temperature (K). For an adsorption process to be controlled chemically (chemisorption), the typical bonding energy should be in the range of 8–16 kJ mol^{-1}. Conversely, if it was controlled physically (physisorption), the adsorption energy should be less than

−40 kJ mol^{-1}.[25] Thus, the b_T value obtained (0.091 kJ mol^{-1}) indicates rather weak ion interaction between Cr(VI) ions and the NFe_3O_4Starch-Glu-NFe_3O_4ED nanocomposite *via* the physisorption process. In addition, the identified R^2 value (Table S4 and Fig. S6c, (ESI†)) reveals that the isotherm data for Cr(VI) adsorption on the NFe_3O_4Starch-Glu-NFe_3O_4ED nanocomposite is best fitted to the Temkin isotherm model among the investigated isotherm models (R^2 = 0.9927).

Moreover, the equilibrium of Cr(VI) was also investigated and monitored in relation to the Dubinin–Radushkevich (D–R) isotherm. Calculating the value of the sorption energy in this model (E_s in kJ mol^{-1}) is very helpful to predict the mechanistic type of adsorption, which it can be directly calculated using eqn (5).

$$E_s = \frac{1}{\sqrt{2K_{ad}}} \quad (5)$$

If the magnitude of E_s is less than 8 kJ mol^{-1}, physical adsorption will take place, whereas in the case of chemisorption or ion exchange, the value of E_s will fall in the range of 8–16 kJ mol^{-1}.[44,48] The value of E_s in the present study was 0.047 kJ mol^{-1}, representing a physisorption process.[44] However, as shown in Table S4 and Fig. S6d (ESI†), the experimental data does not match the D–R isotherm model (R^2 value = 0.8920). The adsorption reaction equilibrium of Cr(VI) ions on the NFe_3O_4Starch-Glu-NFe_3O_4ED nanocomposite was found to follow the fitting order of Temkin > Langmuir > Freundlich > D–R according to the correlation coefficients.

3.2.5. The effect of reaction temperature on Cr(VI) adsorption and thermodynamic parameters. The influence of reaction temperature on the adsorption and removal of various toxic heavy metals was reported in previous studies.[45,47] Usually this type of study includes changing the reaction temperature to determine the effect of this variation on the sorption process. It also indicates whether sorption has an exothermic or endothermic nature.[45] The adsorptive removal percentage of Cr(VI) on NFe_3O_4Starch-Glu-NFe_3O_4ED was tested in the temperature range of 20 °C to 60 °C and the collected results are plotted graphically in Fig. S7 (ESI†). For the three concentrations under investigation, the adsorptive removal percentage of Cr(VI) on the NFe_3O_4Starch-Glu-NFe_3O_4ED nanocomposite was found to increase as the reaction temperature increased. This trend confirms that the adsorption process of Cr(VI) on NFe_3O_4Starch-Glu-NFe_3O_4ED follows an endothermic interaction mechanism. The maximum adsorptive removal percentage values for Cr(VI) were characterized to be 83.87%, 86.61%, and 85.88% using 10.0, 25.0, and 50.0 mg L^{-1} of Cr(VI), respectively, at 60 °C, as displayed in Fig. S7 (ESI†). This shows that the newly developed NFe_3O_4Starch-Glu-NFe_3O_4ED nanocomposite can extract and remove Cr(VI) ions from aqueous solution in a wide reaction temperature range.

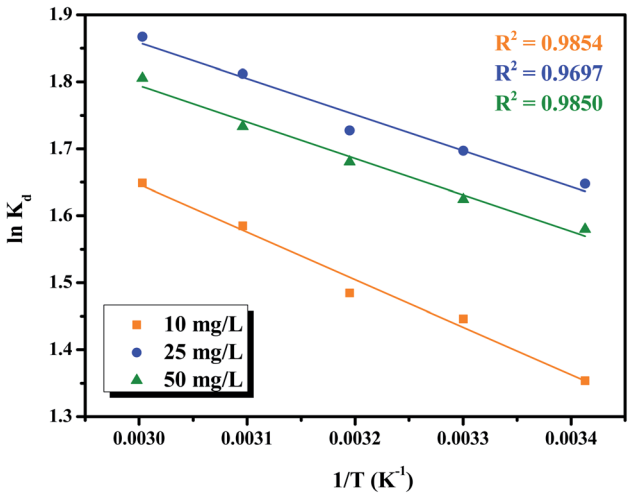

Fig. 5 Van't Hoff plot for the adsorptive removal of Cr(VI) ions (concentration = 10.0, 25.0, and 50.0 mg L^{-1}) on the NFe_3O_4Starch-Glu-NFe_3O_4ED nanocomposite.

Table 1 Standard thermodynamic parameters for the adsorption of Cr(VI) on the NFe_3O_4Starch-Glu-NFe_3O_4ED nanocomposite at different reaction temperatures

Initial concentration of Cr(VI) (mg L^{-1})	Temperature (K)	ln K_d (L g^{-1})	Adsorption thermodynamic parameters			R^2
			ΔG° (kJ mol^{-1})	ΔH° (kJ mol^{-1})	ΔS° (J mol^{-1} K^{-1})	
10.0	293	1.65	**−3.297**	5.908	31.410	0.9854
	303	1.70	**−3.643**			
	313	1.73	**−3.863**			
	323	1.81	**−4.256**			
	333	1.87	**−4.564**			
25.0	293	1.65	**−4.013**	4.472	28.866	0.9697
	303	1.70	**−4.275**			
	313	1.73	**−4.495**			
	323	1.81	**−4.865**			
	333	1.87	**−5.169**			
50.0	293	1.58	**−3.849**	4.526	28.492	0.9850
	303	1.62	**−4.092**			
	313	1.68	**−4.373**			
	323	1.73	**−4.655**			
	333	1.81	**−4.998**			

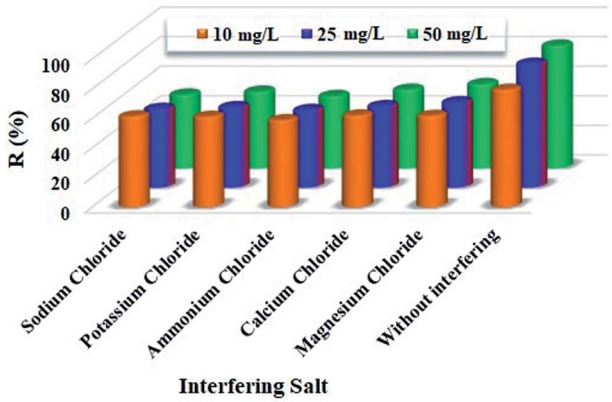

Fig. 6 .Effect of interfering species on Cr(VI) ion removal percentage (%*R*) by the NFe_3O_4Starch-Glu-NFe_3O_4ED nanocomposite. (Sample volume = 10.0 mL; nanosorbent dose = 10.0 ± 1 mg; Cr(VI) initial concentrations = 10.0, 25.0, and 50.0 mg L; pH value = 2.0; shaking time = 60.0 min; temperature = 25 °C; mass of interfering salt = 100.0 ± 0.1 mg; shaking speed = 250 rpm).

To evaluate the heat change and determine whether the adsorption of Cr(VI) by the NFe_3O_4Starch-Glu-NFe_3O_4ED nanocomposite is spontaneous or not, it was important to consider the thermodynamics of the process. The Gibbs free energy change (ΔG°), enthalpy change (ΔH°), and entropy change (ΔS°), all considered thermodynamic parameters, were calculated from the experimental adsorption equilibrium data measured at different reaction temperatures, as listed in Table 1. These parameters were calculated using eqn (6)–(8).[25]

$$\Delta G^\circ = -RT \ln K_d \quad (6)$$

$$\Delta G^\circ = \Delta H^\circ - T\Delta S^\circ \quad (7)$$

$$\ln K_d = \frac{\Delta S^\circ}{R} - \frac{\Delta H^\circ}{RT} \quad (8)$$

where T is the absolute temperature (K) and K_d (L g^{-1}) is the adsorption equilibrium constant, which was calculated using eqn (9).

$$K_d = \frac{q_e}{C_e} \quad (9)$$

where q_e (mg g^{-1}) is the quantity of Cr(VI) adsorbed onto NFe_3O_4Starch-Glu-NFe_3O_4ED at equilibrium and C_e (mg L^{-1}) is the concentration of Cr(VI) at equilibrium. According to Fig. 5, the values of ΔH° and ΔS° were calculated using the slope and intercept of the linear Van't Hoff plot of ln K_d *vs.* $1/T$, respectively. All the calculated results are listed in Table 1. Fig. 5 demonstrates that all the points of the relation between the adsorption equilibrium constants over the selected experimental temperature range lie on a straight line. This means that Cr(VI) ions bind to the same interaction sites on the NFe_3O_4-Starch-Glu-NFe_3O_4ED nanocomposite.[45] The negative values identified for ΔG° confirm that the process of adsorption of Cr(VI) on NFe_3O_4Starch-Glu-NFe_3O_4ED is thermodynamically feasible and that the nanocomposite spontaneously adsorbs Cr(VI) with high selectively. Additionally, the values of ΔG° were found to increase in magnitude from 3.297 to 4.564 kJ mol^{-1}, from 4.013 to 5.169 kJ mol^{-1}, and from 3.849 to 4.998 kJ mol^{-1} for the three concentrations tested of Cr(VI), *i.e.*, 10.0, 25.0, and 50.0 mg L^{-1}, respectively, as the reaction temperature increased from 20 °C to 60 °C. This indicates that increasing the temperature enhanced the adsorption between Cr(VI) ions and the assembled nanocomposite due to the increasing number of available active sites for the adsorption process as well as the decrease in the boundary layer surrounding the NFe_3O_4Starch-Glu-NFe_3O_4ED nanocomposite.[45] Conversely, the identified positive values of ΔH° (5.908, 4.472, and 4.526 kJ mol; all <25 kJ mol^{-1}) indicate that the adsorption reaction of Cr(VI) ions on the NFe_3O_4Starch-Glu-NFe_3O_4ED nanocomposite is endothermic and physical in nature.[25] Besides, the values of ΔS° (Fig. 5) were determined to be 31.410, 28.866, and 28.492 J mol^{-1} K^{-1} for 10.0, 25.0, and 50.0 mg L^{-1} of Cr(VI) ions concentrations, respectively. The positive values identified for ΔS° reflects an increase in the randomness at the solid/solution interface during the adsorption process that caused by the release of water molecules around Cr(VI) with some structural changes in the NFe_3O_4Starch-Glu-NFe_3O_4ED nanocomposite.[25,45]

3.2.6. The effect of interfering ions. The adsorption characteristics of a sorbent for metal ions are generally dependent on the type and concentration of other co-existing and competing ions which are present in the liquid phase.

Table 2 Adsorptive removal of Cr(VI) ions from real samples by the NFe_3O_4Starch-Glu-NFe_3O_4ED nanocomposite[a]

	% Removal									
	1st run			2nd run			3rd run			
	10.0 mg L^{-1}	25.0 mg L^{-1}	50.0 mg L^{-1}	10.0 mg L^{-1}	25.0 mg L^{-1}	50.0 mg L^{-1}	10.0 mg L^{-1}	25.0 mg L^{-1}	50.0 mg L^{-1}	Conditions
Tap water	83.71	85.97	86.65	91.23	92.78	95.97	—	—	—	Shaking time = 30.0 min, pH = 2.0, nanosorbent mass = 40.0 ± 1.0 mg
Sea water	79.18	83.81	84.73	86.63	86.79	87.78	91.77	92.36	94.67	
Wastewater	81.37	84.16	85.62	90.14	91.75	94.63	—	—	—	

[a] Values are based on triplicate analysis.

Table 3 Comparison with other previously reported nanosorbents

Adsorbent	Maximum adsorption capacity q_{max} (mg g^{-1})	pH	Equilibrium time (min)	Reference
NFe_3O_4Starch-Glu-NFe_3O_4ED nanocomposite	210.741	2.0	30.0	This work
EDA-MPs-2	32.150	2.5	5.0	29
EDA-MPs-4	36.630	2.5	10.0	
EDA-MPs-6	49.500	2.5	30.0	
EDA-MPs-8	60.980	2.5	60.0	
EDA-MPs-10	61.350	2.5	60.0	
Ethylenediamine-modified cross-linked magnetic chitosan	51.813	2.0	60.0	25
Modified $MnFe_2O_4$	31.550	2.0	5.0	49
Poly(GMA-co-MMA)-ED	22.900	2.0	120.0	50
Lignin	5.640	3.0	>600.0	51
Starch functionalized iron oxide nanoparticles (IONPs)	9.020	2.0	1440.0	14
Fe@Fe_2O_3 core–shell nanowires	7.780	3.0	120.0	52
Fe_3O_4–polyethylenimine–montmorillonite	8.800	3.0	120.0	53
NFe_3O_4@MIL-88A(Fe)/APTMS	7.990	2.0	30.0	54
Fe_3O_4–GS	17.290	2.0	240.0	28

Moreover, the selectivity of a sorbent for certain metal ion is also based on its selectivity towards other competing ions. Therefore, the adsorptive removal percentage values of Cr(VI) by NFe_3O_4Starch-Glu-NFe_3O_4ED were also investigated and determined in the presence of other competing metal ions, such as K^+, NH_4^+, Na^+, Ca^{2+}, and Mg^{2+}as well as without interference. Fig. 6 shows the collected results of this study in the presence and absence of competing metal ions. Selection of these cations is mainly due to their expected existence in various water samples such as wastewater, drinking water and sea water. Noticeable changes in the removal process of Cr(VI) on the NFe_3O_4Starch-Glu-NFe_3O_4ED nanocomposite were evident as a result of the presence of the co-existing species. The presence of these metal ions in solution was found to contribute to a significant decrease in the removal percentage for the three evaluated Cr(VI) concentrations compared with the removal percentage values without competing ions. The examined interfering metal ions can be grouped in the ascending order of interference of Mg^{2+} < Ca^{2+} < K^+ < Na^+< NH_4^+ for the three investigated Cr(VI) concentrations (Fig. 6). This trend proves that NH_4^+ is the highest interfering species in the sorption process of Cr(VI) by the NFe_3O_4Starch-Glu-NFe_3O_4ED nanocomposite, whose presence led to lower removal percentages (85.72%, 52.49%, and 48.93% using 10.0, 25.0, and 50.0 mg L^{-1} of Cr(VI), respectively). These results are related to the fact that NH_4^+ exhibits the highest competing behavior with Cr(VI) among the selected coexisting ions, binding to the active surface functional groups on the NFe_3O_4Starch-Glu-NFe_3O_4ED nanocomposite. Generally, the ionic radii and ionic charge of the interfering ions as well as the nature of the functional groups on the surface of the nanocomposite are the main reasons for the competitive affinity between the target metal ions (Cr(VI)) and the interfering ions on the surface of the NFe_3O_4Starch-Glu-NFe_3O_4ED nanocomposite as previously reported.[44,45]

3.2.7. Potential application of NFe_3O_4Starch-Glu-NFe_3O_4-ED nanocomposite for the removal of Cr(VI) from real water matrices. The application of the newly designed NFe_3O_4Starch-Glu-NFe_3O_4ED nanocomposite for the adsorptive removal of Cr(VI) ions from real water matrices is an important final step performed in this study *via* batch equilibrium technique. The selected water samples were spiked with 10.0, 25.0, and 50.0 mg L^{-1} of Cr(VI) and then adjusted to the optimum conditions for the extraction and the adsorptive removal process. The collected data of this study is presented in Table 2. The adsorptive removal percentage values of Cr(VI) were determined to be 91.2 ± 3.0%, 92.8 ± 2.2% and 95.9 ± 3.1% (tap water), 90.1 ± 3.3%, 91.8 ± 2.6% and 94.6 ± 3.4% (wastewater), 91.8 ± 3.0%, 92.4 ± 2.6% and 94.7 ± 3.7% (sea water) for the samples spiked with 10.0, 25.0 and 50.0 mg L^{-1} of Cr(VI) ions, respectively. Thus, the outlined results in this section confirm the validity and applicability of the NFe_3O_4Starch-Glu-NFe_3O_4-ED hybrid nanocomposite for the effective adsorption of Cr(VI) ions from different water sources.

4. Conclusion

A strategy was employed in this study to synthesize a newly designed magnetic NFe_3O_4Starch-Glu-NFe_3O_4ED nanocomposite and verify its characteristics for the successful removal of Cr(VI) from aqueous solution. The sorption process and experimental controlling parameters were tested, and the optimized values of each parameter were determined using the batch adsorption technique. The maximum percentage values of Cr(VI) removal were identified at pH 2.0, while shaking for a period of 30.0 min using 40.0 mg of the NFe_3O_4Starch-Glu-NFe_3O_4ED nanocomposite to establish 85.27%, 91.90%, and 96.47% removal by 10.0, 25.0 and 50.0 mg L^{-1} of Cr(VI), respectively. The studied and evaluated kinetic models confirmed the valid fitting of the adsorption of Cr(VI) ions on the NFe_3O_4Starch-Glu-NFe_3O_4ED nanocomposite according to the pseudo-second-order (R^2 = 0.9997) and Elovich (R^2 = 0.9706) isotherm models based on an ion-pair interaction mechanism. The equilibrium data was correlated well with the Temkin

model followed by the Langmuir model compared to the other isotherm models. The dependence of Cr(VI) adsorption on temperature revealed that the adsorption process was characterized by feasibility, spontaneity and endothermic nature. The mechanism of adsorption of Cr(VI) on NFe_3O_4Starch-Glu-NFe_3O_4ED was mainly based on the ion-pair interaction occurring between the negatively charged $HCrO_4^-$ and $Cr_2O_7^{2-}$ and the positively charged magnetic NFe_3O_4Starch-Glu-NFe_3O_4ED nanocomposite at lower pH. Certain ions, such as Na^+, K^+, Ca^{2+}, Mg^{2+}, and NH_4^+ were found to exhibit strong interference in the process of Cr(VI) removal from water. The investigated NFe_3O_4-Starch-Glu-NFe_3O_4ED was confirmed as a promising nanocomposite for the removal of Cr(VI) from different real water samples. Finally, the developed magnetic NFe_3O_4Starch-Glu-NFe_3O_4ED nanocomposite was found to display excellent values of adsorptive removal percentage of Cr(VI) compared to other previously reported adsorbents under the same experimental conditions (Table 3).

Conflicts of interest

There are no conflicts to declare.

References

1 V. E. Pakade, N. T. Tavengwab and L. M. Madikizela, Recent advances in hexavalent chromium removal from aqueous solutions by adsorptive methods, *RSC Adv.*, 2019, **9**, 26142.

2 P. C. Grevatt, *Toxicological Review of Hexavalent Chromium, Support of Summary Information on the Integrated Risk Information System (IRIS)*, US Environmental Protection Agency, Washington DC, US, 1998.

3 E. A. Allam, R. M. El-Sharkawy, M. A. Gizawy and M. E. Mahmoud, Assembly of CeO_2–MoO_3–$SiO_2(CH_2)_3$–$(Alginate)_2$ as a novel nanocomposite for removal of Mn^{II}/Cr^{VI} and $^{56}Mn/^{51}Cr$ radionuclides from water, *Mater. Chem. Phys.*, 2021, **262**, 124278.

4 J. Bayuo, K. B. Pelig-Ba and M. A. Abukari, Adsorptive removal of chromium(VI) from aqueous solution unto groundnut shell, *Appl. Water Sci.*, 2019, **9**, 107.

5 A. Assadi, M. H. Dehghani, N. Rastkari, S. Nasseri and A. H. Mahvi, Photocatalytic reduction of hexavalent chromium in aqueous solutions with zinc oxide nanoparticles and hydrogen peroxide, *Environ. Prot. Eng.*, 2012, **38**, 4–16.

6 *Independent Environmental Technical Evaluation Group (IETEG), Chromium(VI) Handbook*, CRC Press, 2005.

7 V. Gómez and M. P. Callao, Chromium determination and speciation since 2000, *Trends Anal. Chem.*, 2006, **25**, 1006–1015.

8 L. M. Calder, *Chromium Contamination of Groundwater*, John Wiley & Sons, New York, 1988, pp. 215–230.

9 M. Cieslak-Golonka, Toxic and mutagenic effects of chromium(VI), *Polyhedron*, 1996, 3667–3689.

10 World Health Organization, *Chromium in Drinking-Water – Background 702 Document for Development of WHO Guidelines for Drinking-Water Quality, 703*, WHO, Geneva, Switzerland, 2003.

11 S. Sharifi, R. Nabizadeh, B. Akbarpour, A. Azari, H. R. Ghaffari, S. Nazmara, B. Mahmoudi, L. Shiri and M. Yousefi, Modeling and optimizing parameters affecting hexavalent chromium adsorption from aqueous solutions using Ti-XAD7 nanocomposite: RSM-CCD approach, kinetic, and isotherm studies, *J. Environ. Health Sci. Eng.*, 2019, **17**, 873–888.

12 P. N. Singh, D. Tiwary and I. Sinha, Improved removal of Cr(VI) by starch functionalized iron oxide nanoparticles, *J. Environ. Chem. Eng.*, 2014, **2**, 2252–2258.

13 D. Park, How to study Cr(VI) biosorption: use of fermentation waste for detoxifying Cr(VI) in aqueous solution, *Chem. Eng. J.*, 2008, **136**, 173–179.

14 S. Rengaraj, K. H. Yeon and S. H. Moon, Removal of chromium from water and wastewater by ion exchange resins, *J. Hazard. Mater.*, 2001, **87**, 273–287.

15 T. Mohammadi, A. Moheb, M. Sadrzadeh and A. Razmi, Modeling of metal ion removal from wastewater by electrodialysis, *Sep. Purif. Technol.*, 2005, **41**, 73–82.

16 R. M. El-Sharkawy, E. A. Allam and M. E. Mahmoud, Functionalization of CeO_2-SiO_2-$(CH_2)_3$-Cl nanoparticles with sodium alginate for enhanced and effective Cd^{II}, Pb^{II}, and Zn^{II} ions removal by microwave irradiation and adsorption technique, *Environ. Nanotechnol. Monit. Manag.*, 2020, **14**, 100367.

17 A. R. Asgari, F. Vaezi, S. Nasseri, O. Dordelmann, A. H. Mahvi and E. D. Fard, Removal of hexavalent chromium from drinking water by granular ferric hydroxide, *Iran. J. Environ. Health. Sci. Eng.*, 2008, **5**, 277–282.

18 E. Bazrafshan, A. H. Mahvi, S. Naseri and A. R. Mesdaghinia, Performance Evaluation of Electrocoagulation Process for Removal of Chromium(VI) from Synthetic Chromium Solutions Using Iron and Aluminum Electrodes, *Turk. J. Eng. Environ. Sci.*, 2008, **32**, 59–66.

19 G. Sharma, M. Naushad, A. A. H. Al-Muhtaseb, A. Kumar, M. R. Khan, S. Kalia, M. Shweta and A. S. Bala, Fabrication and characterization of chitosan crosslinked-poly(alginic acid) nanohydrogel for adsorptive removal of Cr(VI) metal ion from aqueous medium, *Int. J. Biol. Macromol.*, 2017, **95**, 484–493.

20 K. Z. Elwakeel, A. Shahat, A. S. Al-Bogami, B. Wijesiri and A. Goonetilleke, The synergistic effect of ultrasound power and magnetite incorporation on the sorption/desorption behavior of Cr(VI) and As(V) oxoanions in an aqueous system, *J. Colloid Interface Sci.*, 2020, **569**, 76–88.

21 M. G. Warner, C. L. Warner, R. S. Addleman and W. Yantasee, *Magnetic Nanomaterials for Environmental Applications, Nanotechnologies for the Life Sciences*, 2009.

22 H. Kazemzadeh, A. Ataie and F. Rashchi, Synthesis of magnetite nano-particles by reverse co precipitation, *Int. J. Mod. Phys.: Conf. Ser.*, 2012, **5**, 160–167.

23 W. Wu, Q. He and C. Jiang, Magnetic iron oxide nanoparticles: synthesis and surface functionalization strategies, *Nanoscale Res. Lett.*, 2008, **3**, 397–415.

24 M. Bhaumik, A. Maity, V. V. Srinivasu and M. S. Onyango, Enhanced removal of Cr(VI) from aqueous solution using polypyrrole/Fe_3O_4 magnetic nanocomposite, *J. Hazard. Mater.*, 2011, **190**, 381–390.

25 X. Hu, J. Wang, Y. Liu, X. Li, G. Zeng, Z. Bao, X. Zeng, A. Chen and F. Long, Adsorption of chromium(VI) by ethylenediamine-modified cross-linked magnetic chitosan resin: isotherms, kinetics and thermodynamics, *J. Hazard. Mater.*, 2011, **185**, 306–314.

26 X. Lv, Y. Hu, J. Tang, T. Sheng, G. Jiang and X. Xu, Effects of co-existing ions and natural organic matter on removal of chromium(VI) from aqueous solution by nanoscale zero valent iron (nZVI)-Fe_3O_4 nanocomposites, *Chem. Eng. J.*, 2013, **218**, 55–64.

27 Y. G. Zhao, H. Y. Shen, S. D. Pan, M. Q. Hu and Q. H. Xia, Preparation and characterization of amino-functionalized nano-Fe_3O_4 magnetic polymer adsorbents for removal of chromium(VI) ions, *J. Mater. Sci.*, 2010, **45**, 5291–5301.

28 X. Guo, B. Du, Q. Wei, J. Yang, L. Hu, L. Yan and W. Xu, Synthesis of amino functionalized magnetic graphenes composite material and its application to remove Cr(VI), Pb(II), Hg(II), Cd(II) and Ni(II) from contaminated water, *J. Hazard. Mater.*, 2014, **278**, 211–220.

29 Z. Y. Gang, S. H. Yua, P. S. Dong and H. M. Qin, Synthesis, characterization and properties of ethylenediamine-functionalized Fe_3O_4 magnetic polymers for removal of Cr(VI) in wastewater, *J. Hazard. Mater.*, 2010, **182**, 295–302.

30 J. Zhu, S. Wei, H. Gu, S. B. Rapole, Q. Wang, Z. Luo, N. Haldolaarachchige, D. P. Young and Z. Guo, One-Pot Synthesis of Magnetic Graphene Nanocomposites Decorated with Core@Double-shell Nanoparticles for Fast Chromium Removal, *Environ. Sci. Technol.*, 2012, **46**, 977–985.

31 H. Liu, P. Li, T. Zhang, Y. Zhu and F. Qiu, Fabrication of recyclable magnetic double-base aerogel with waste bioresource bagasse as the source of fiber for the enhanced removal of chromium ions from aqueous solution, *Food Bioprod. Process.*, 2020, **119**, 257–267.

32 M. Nasrollahzadeh, N. Shafiei, Z. Nezafat, N. S. S. Bidgoli and F. Soleimani, Recent progresses in the application of cellulose, starch, alginate, gum, pectin, chitin and chitosan based (nano)catalysts in sustainable and selective oxidation reactions: A review, *Carbohydr. Polym.*, 2020, **241**, 116353.

33 A. O. Ashogbon and E. T. Akintayo, Recent trend in the physical and chemical modification of starches from different botanical sources: a review, *Starch-Starke*, 2014, **66**, 41–57.

34 G. Xing, S. Zhang, B. Ju and J. Yang, Study on adsorption behavior of crosslinked cationic starch maleate for chromium(VI), *Carbohydr. Polym.*, 2006, **66**, 246–251.

35 K. Baek, J. S. Yang, T. S. Kwon and J. W. Yang, Cationic starch-enhanced ultrafiltration for Cr(VI) removal, *Desalination*, 2007, **206**, 245–250.

36 H. Kolya, A. Roy and T. Tripathy, Starch-g-poly-(N, N-dimethyl acrylamide-co-acrylic acid): an efficient Cr(VI) ion binder, *Int. J. Biol. Macromol.*, 2015, **72**, 560–568.

37 S. S. Pillai, M. D. Mullassery, N. B. Fernandez, N. Girija, P. Geetha and M. Koshy, Biosorption of Cr(VI) from aqueous solution by chemically modified potato starch: equilibrium and kinetic studies, *Ecotoxicol. Environ. Saf.*, 2013, **92**, 199–205.

38 A. A. Dong, Novel method for amino starch preparation and its adsorption for Cu(II) and Cr(VI), *J. Hazard. Mater.*, 2010, **81**, 448–454.

39 M. E. Mahmoud, M. F. Amira, A. A. Zaghloul and G. A. A. Ibrahim, Microwave-enforced sorption of heavy metals from aqueous solutions on the surface of magnetic iron oxide-functionalized-3-aminopropyltriethoxysilane, *Chem. Eng. J.*, 2016, **293**, 200–206.

40 K. A. Stancheva, B. I. Bogdanov, D. P. Georgiev, Y. H. Hristov and I. G. Markovska, Spectrophotometric Determination of Hexavalent Chromium Content in Commercial Cement – An Assessment of the Optimal Conditions for the Analysis of Chromium(VI), *Eurasian J. Anal. Chem.*, 2013, **8**, 10–16.

41 M. E. Mahmoud, M. F. Amira, A. A. Zaghloul and G. A. A. Ibrahim, High performance microwave-enforced solid phase extraction of heavy metals from aqueous solutions using magnetic iron oxide nanoparticles protected-nanosilica, *Sep. Purif. Technol.*, 2016, **163**, 169–172.

42 M. E. Mahmoud, G. A. A. Ibrahim and M. S. Abdelwahab, Manganese dioxide nanoparticles decorated with chitosan for effective removal of lead and lanthanum ions from water by microwave sorption technique, *Mater. Sci. Eng., B*, 2021, **267**, 115091.

43 M. E. Mahmoud, E. A. Allam, R. M. El-Sharkawy, M. A. Soliman, E. A. Saad and A. M. El-Khatib, Nano-manganese oxide-functionalized-oleyl amine as a simple and low cost nanosorbent for remediation of Zn^{II}/Co^{II} and their radioactive nuclides ^{65}Zn and ^{60}Co from water, *Appl. Radiat. Isot.*, 2020, **159**, 108989.

44 M. E. Mahmoud, G. M. Nabil, M. M. Zaki and M. M. Saleh, Starch functionalization of iron oxide by-product from steel industry as a sustainable low cost nanocomposite for removal of divalent toxic metal ions from water, *Int. J. Biol. Macromol.*, 2019, **137**, 455–468.

45 M. E. Mahmoud, N. A. Fekry and A. M. Abdelfattah, Removal of uranium (VI) from water by the action of microwave-rapid green synthesized carbon quantum dots from starch-water system and supported onto polymeric matrix, *J. Hazard Mater.*, 2020, 397–122770.

46 K. Z. Elwakeel, A. M. Elgarahy, Z. A. Khan, M. S. Almughamisia and A. S. Al-Bogami, Perspectives regarding metal/mineral-incorporating materials for water purification: with special focus on Cr(VI) removal, *Mater. Adv.*, 2020, **1**, 1546–1574.

47 Y. A. Aydın and N. D. Aksoy, Adsorption of chromium on chitosan: optimization, kinetics and thermodynamics, *Chem. Eng. J.*, 2009, **151**, 188–194.

48 L. B. Almalike, Equations Adsorption Isotherms for Biuret on Soils, Paper and Cortex Plant Application of the Freundlich, Langmuir, Temkin, Elovich, Flory-Huggins,

Halsey, and Harkins-Jura, *Int. J. Adv. Res. Chem. Sci.*, 2017, **4**, 9–20.

49 J. Hu, I. M. C. Lo and G. H. Chen, Fast removal and recovery of Cr(VI) using surface-modified jacobsite ($MnFe_2O_4$) nanoparticles, *Langmuir*, 2005, **21**, 11173–11179.

50 G. Bayramoglu and M. Y. Arıca, Ethylenediamine grafted poly (glycidylmethacrylate-co-methylmethacrylate) adsorbent for removal of chromate anions, *Sep. Purif. Technol.*, 2005, **45**, 192–199.

51 S. B. Lalvani, A. Hubener and T. S. Wiltowski, Chromium adsorption by lignin, *Energy Sources*, 2000, **22**, 45–56.

52 Z. Ai, Y. Cheng, L. Zhang and J. Qiu, Efficient removal of Cr(VI) from aqueous solution with Fe@Fe_2O_3 core–shell nanowires, *Environ. Sci. Technol.*, 2008, **42**, 6955–6960.

53 I. Larraza, M. López-Gónzalez, T. Corrales and G. Marcelo, Hybrid materials: magnetite polyethylenimine–montmorillonite, as magnetic adsorbents for Cr(VI) water treatment, *J. Colloid Interface Sci.*, 2012, **385**, 24–33.

54 M. E. Mahmoud, M. F. Amira, S. M. Seleim and A. K. Mohamed, Amino-decorated magnetic metal-organic framework as a potential novel platform for selective removal of chromium (VI), cadmium (II) and lead (II), *J. Hazard. Mater.*,, 2020, **381**, 120979.